



Synthesis of N-doped carbon with embedded Fe/Fe₃C particles for microwave absorption

Yingchun Niu¹, Xueai Li^{1,*}, Wenqi Dong¹, Can Zhang¹, Kuihu Zhao¹, Fengyan Wang¹, and Haiyan Wang^{1,*}

¹ Hebei Key Laboratory of Applied Chemistry, Hebei Key Laboratory of Heavy Metal Deep-Remediation in Water and Resource Reuse, College of Environment and Chemical Engineering, Yanshan University, No. 438 Hebei Street, Haigang District, Qinhuangdao 066004, People's Republic of China

Received: 26 December 2019

Accepted: 7 June 2020

Published online:

16 June 2020

© Springer Science+Business Media, LLC, part of Springer Nature 2020

ABSTRACT

Carbon and iron composites have drawn much attention for their unique electromagnetic properties. In addition, nitrogen doping of carbon can effectively modulate the dielectric properties of carbon. Therefore, synthesis of N-doped carbon and iron composites is an alternative method for obtaining high-efficiency microwave absorption materials. In previous studies, the synthesis process was very complicated including multistep routes. In this work, N-doped carbon with embedded Fe/Fe₃C was synthesized in-situ via pyrolysis of amino phenol formaldehyde resin (APF) scattered with Fe₂O₃ nanoparticles (APF/Fe₂O₃), which was obtained through a simple hydrothermal process. During the heat-treatment process, the APF resin was converted into N-doped carbon, and simultaneously, the Fe₂O₃ was reduced to iron nanoparticles. Then, inevitably, the iron nanoparticles reacted with carbon to form Fe₃C at the interface between the iron particles and carbon. Taking advantage of multiple heterogenous interface, the interfacial polarization relaxation could be enhanced. Therefore, the N-doped carbon with embedded Fe/Fe₃C particles displays microwave absorption with a maximum reflection loss of – 70 dB. Moreover, the effective absorption bandwidth (reflection loss of less than – 10 dB) reaches 6.02 GHz at a thickness of 2.13 mm. This study not only provides composites of N-doped carbon with embedded Fe/Fe₃C particles with excellent stable microwave absorption but also offers a simple method for synthesizing N-doped carbon with embedded Fe/Fe₃C particles.

Address correspondence to E-mail: lixueai@ysu.edu.cn; hywang@ysu.edu.cn

Introduction

With the widespread application of electromagnetic devices, the adverse effects of electromagnetic pollution on ecosystems have become increasingly serious [1–3]. The application of microwave absorption materials (MAMs) is an effective way to solve the above problem. MAMs must possess the characteristics of strong absorption, wide effective absorption bandwidth, light weight and small thickness in practical applications [4–6]. In fact, the microwave absorption characteristics of MAMs are mainly determined by their attenuation and impedance matching. Impedance matching controls the entrance of microwave into the material, while attenuation determines the dissipation of the microwave energy [7–9].

Among MAMs, carbon materials, such as carbon nanofiber [10, 11], carbon nanotube [12, 13], and graphene [14–16], are widely investigated for their light weight, good chemical stability, excellent dielectric properties and tunable properties [17–19]. However, the microwave absorption performance of traditional pure carbon materials is always restricted, and it is challenging to achieve strong absorption and wide bandwidth. To improve the microwave absorption ability of carbon materials, creating a hierarchical structure is a promising method. A hierarchical structure not only modifies the density of materials but also can provide more opportunities for interaction between the microwave and absorber [20–22]. Consequently, the attenuation of microwave will be strengthened through multi-absorption and scattering of incident microwave [23, 24]. Furthermore, recent studies have indicated that defects are generated by N atoms-doping in graphene, which can tune the physical and chemical properties of carbon [25, 26]. Therefore, synthesizing N-doped carbon materials with defect states is a promising way to improve the microwave absorption performance [27, 28]. For example, Zhou et al. reported the doping of a three-dimensional graphene lattice with nitrogen atoms, which could greatly improve the dielectric loss [28]. However, the improvement of microwave absorption performance of carbon materials is limited by modifying the carbon structure or forms. Moreover, in addition to the dielectric and resistance loss of carbon materials, the microwave energy can be attenuated by magnetic loss [27–31]. In

the latest research, constructing composites of carbon materials decorated with ferromagnetic particles is a well-established means to synthesize MAMs with desirable microwave absorption [32–35]. Remarkably, Liu et al. reported that porous carbon decorated with even low Fe content can exhibit excellent microwave absorption performance with an optimal reflection loss of -29.5 dB at a thickness of 2.5 mm [36]. In other studies, it has been found that various N-doped carbon materials decorated by ferromagnetic metals present enhanced microwave absorption performance [37–41]. Liu et al. described the synthesis of N-doped carbon nanofibers decorated with cobalt nanoparticles, which presented the maximum reflection loss of -25.7 dB at a thickness of 2 mm and effective bandwidth (reflection loss over -10 dB) of 4.3 GHz [42]. Yuan et al. researched the influence of nickel and nitrogen contents on the electromagnetic properties of nickel encapsulated nitrogen-doped graphite sheets. The composites with the optimized Ni content exhibited a maximum microwave absorption of -45 dB with a thickness of 4.0 mm [43].

The common methods for synthesizing porous carbon and ferromagnetic metal composites generally involve multistep and template-using approaches, that require presynthesis and complicated insertion and removal procedures [18, 24, 41]. Herein, porous N-doped carbon with embedded Fe/Fe₃C nanoparticles was synthesized in-situ through heat treatment of amino phenol formaldehyde resin scattered with iron oxide nanoparticles obtained by a simple hydrothermal process. The synthesis process is schematically illustrated in Fig. 1. 3-Aminophenol (3-AP), hexamethylenetetramine (HMT) and FeCl₃·6H₂O were simultaneously dissolved in deionized water, and then the solution was hydrothermally treated. First, HMT decomposed into formaldehyde and ammonia. Then, the formaldehyde reacted with 3-aminophenol under catalysis of ammonia to form the aminophenol formaldehyde (APF) resin. At the

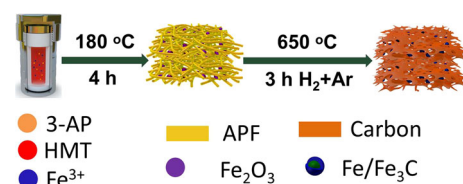


Figure 1 Schematic illustration of the synthesis process of N-doped carbon with embedded Fe/Fe₃C particles.

same time, the Fe^{3+} hydrolyzed and deposited on the APF to form the $\text{Fe}_2\text{O}_3/\text{APF}$ precursor. Finally, the precursor was heat treated under a mixed atmosphere of H_2/Ar (H_2 5 vol%) at 650 °C to prepare composites of N-doped carbon with embedded Fe/ Fe_3C particles. The composites present excellent microwave absorption with an optimal reflection loss of -70 dB. Moreover, it is worth mentioning that the as-synthesized composite exhibits an effective absorption bandwidth of 6.02 GHz with a thickness of 2.13 mm. This work provides a simple method for synthesizing N-doped carbon with embedded Fe/ Fe_3C particles with excellent microwave absorption properties.

Experimental section

Materials

3-Aminophenol (3-AP) and hexamethylenetetramine (HMT) were obtained from Aladdin Reagent (Shanghai) Co. Ltd. Iron chloride hexahydrate ($\text{FeCl}_3 \cdot 6\text{H}_2\text{O}$) was purchased from Shanghai Macklin Biochemical Co., Ltd. All the materials were analytical grade and used without further treatment.

Synthesis

In a typical experiment, 0.22 g (2 mmol) 3-AP, 0.08 g (0.57 mmol) HMT, and 0.38 g (1.4 mmol) $\text{FeCl}_3 \cdot 6\text{H}_2\text{O}$ were simultaneously dissolved in 80 mL deionized water at 30 °C by mechanical stirring, and then the solution was sealed in a 100 ml Teflon-lined stainless autoclave. Then, the autoclave was placed in an oven and kept at 160 °C for 4 h. The solid products were separated and washed by vacuum filtration until the filter liquor was neutral. The obtained samples were dried in a vacuum drying cabinet at 60 °C. To study the influence of additive amounts of Fe^{3+} on the structure and electromagnetic properties, the molar ratios of Fe^{3+} to 3-AP were modified to 0:1, 0.7:1, 1:1 and 2:1. To ensure complete Fe^{3+} decomposition, the usage amount of HMT was adjusted according to the molar ratio of Fe^{3+} to 3-AP. Then, the resultant product was heat treated in a tube furnace under a mixed atmosphere of H_2/Ar (H_2 5 vol%) at 650 °C for 4 h with a heating rate of 1 °C/min. The final Fe/C composites obtained at different molar ratios of Fe^{3+} to 3-AP were defined as Fe/C-0, Fe/C-0.7, Fe/C-1

and Fe/C-2. To study the interfacial polarization between iron and Fe_3C , the iron was removed by etching the Fe/C-0.7 sample in 30 wt% tartaric acid for 8 h and then washed by vacuum filtration until the filter liquor was neutral and dried in an oven at 60 °C to obtain the $\text{Fe}_3\text{C}/\text{C}$ composite.

Characterization

TEM and HRTEM images of the composites were obtained by transmission electron microscopy (TEM, HITACHI HT7700) at 100 kV and high-resolution transmission electron microscopy (HTEM, Tecnai F20) at 200 kV, respectively. The crystalline phases of the materials were recorded by X-ray diffraction (XRD, Rigaku D-max-2500/PC) with a scanning speeds of 0.7 and 2°/min, respectively. Raman spectra were obtained under ambient conditions on a confocal Raman spectroscopic system (Horiba, Xplora Plus). The elements of the sample surface were measured by X-ray photoelectron spectroscopy (XPS, ESCALAB 250 Xi). The Brunauer–Emmett–Teller (BET, ASAP 2020) method was used to analyze the specific surface area of the materials. Thermal gravimetric analysis (TGA) was carried out with a NETZSCHSTA-449C in air at a heating rate of 5 °C/min to 800 °C. The magnetic hysteresis loops were obtained at room temperature through a vibrating sample magnetometer (VSM, Lake Shore 7404). The relative complex permeability and permittivity were obtained from a vector network analyzer (Agilent N5230A) in the frequency range of 2.0–18.0 GHz. The test specimen was made into a ring with an outside diameter of 7.00 mm, an inside diameter of 3.04 mm and a thickness of 2 mm with a mass ratio of Fe/C composite to paraffin of 1:1.

Results and discussion

Diffraction peaks in the XRD patterns (Fig. S1) of all the precursors obtained with Fe^{3+} can be indexed to the standard patterns of Fe_2O_3 (JCPDS No. 33-0664). The XRD pattern of the APF precursor (Fig. S1) without Fe^{3+} indicates a broad peak corresponding to amorphous material. The morphology of the precursor was determined by the addition of Fe^{3+} . As observed in Fig. S2a, the APF precursor consists of microspheres; however, the $\text{Fe}_2\text{O}_3/\text{APF}$ precursor is composed of net-like structures embedded with

nanoparticles. When the reaction system contains Fe^{3+} , hydrolysis consumes some OH^- , which modifies the catalysis of ammonia and ultimately alters the polymerization of formaldehyde and 3-aminophenol, resulting in differences between the morphologies of APF and $\text{Fe}_2\text{O}_3/\text{APF}$. As a typical sample, the $\text{Fe}_2\text{O}_3/\text{APF}$ precursor obtained with a molar ratio of Fe^{3+} to 3-AP of 0.7:1 was studied by XPS. Although the XRD and SEM results indicate that there are Fe_2O_3 particles in the precursor composites, the Fe peaks cannot be observed in XPS (Fig. S3a), and the content of Fe is only 0.29 at%. Therefore, there is virtually no iron on the surface of the precursor due to the Fe_2O_3 particles embedded in the APF matrix and the XPS detectable depth of only several nanometers. The high-resolution XPS spectrum of N 1s suggests the existence of N in only one state of Ph-NH₂ with a binding energy of 399.2 eV (Fig. S3b).

TEM images of Fe/C-0, Fe/C-0.7, Fe/C-1 and Fe/C-2 obtained from heat treatment of the $\text{Fe}_2\text{O}_3/\text{APF}$ precursor are shown in Fig. S4. As observed, Fe/C-0 is still composed of spherical particles with a size of ~ 325 nm (Fig. S4a), indicating that the morphology will not be changed by carbonization of APF. Again, it can be seen that the morphology of the Fe^{3+} -containing composites exhibits a net-like structure embedded with particles (Fig. S4b–d). Compared with the precursor, the size of the particles expands to a certain extent. To observe the details of the

microstructure, a representative TEM image of sample Fe/C-0.7 is shown in Fig. 2a. As shown, the particles are homogeneously dispersed in the net-like carbon matrix. The high magnification of the carbon matrix demonstrates its porous structure, as shown in Fig. 2b, for example, the nanoholes indicated by the arrows. The HRTEM image of the carbon matrix inserted in Fig. 2b indicates that it is turbostratic carbon with short range order [44]. Further observation discloses that the particles are encapsulated by a shell coating. The local magnification of one typical particle (Fig. 2c) clearly indicates the existence of the shell. HRTEM images of the shell and core of particles are shown in Fig. 2d, e that indicate that the interplanar distances of the shell and core are 0.26 nm and 0.20 nm, corresponding to the Fe_3C (200) and $\alpha\text{-Fe}$ (110) crystal planes, respectively. The elemental mapping of Fe/C-0.7 is shown in Fig. 2f. The maps display the distributions of the N, C and Fe within the observed structure. Obviously, Fe is only distributed in the particles, indicating that Fe/ Fe_3C particles are embedded in the nitrogen-doped carbon matrix.

Figure 3a shows the XRD patterns of Fe/C-0.7 and $\text{Fe}_3\text{C}/\text{C}$. It is obvious that Fe/C-0.7 displays the typical diffraction peaks of Fe_3C (JCPDS No. 76-1877) and a wide amorphous peak centered at 23.2° ascribed to short range-order turbostratic carbon. In addition, the three peaks located at 44.6° , 65.0° and

Figure 2 TEM image of sample Fe/C-0.7 (a), TEM image of local magnification of carbon matrix (b) and HRTEM image of carbon matrix (inset), TEM image of local magnification of one particle (c), HRTEM image of shell of particle (d), HRTEM image of core of particle (e), elemental maps of distributions of Fe, N and C in Fe/C-0.7 (f).

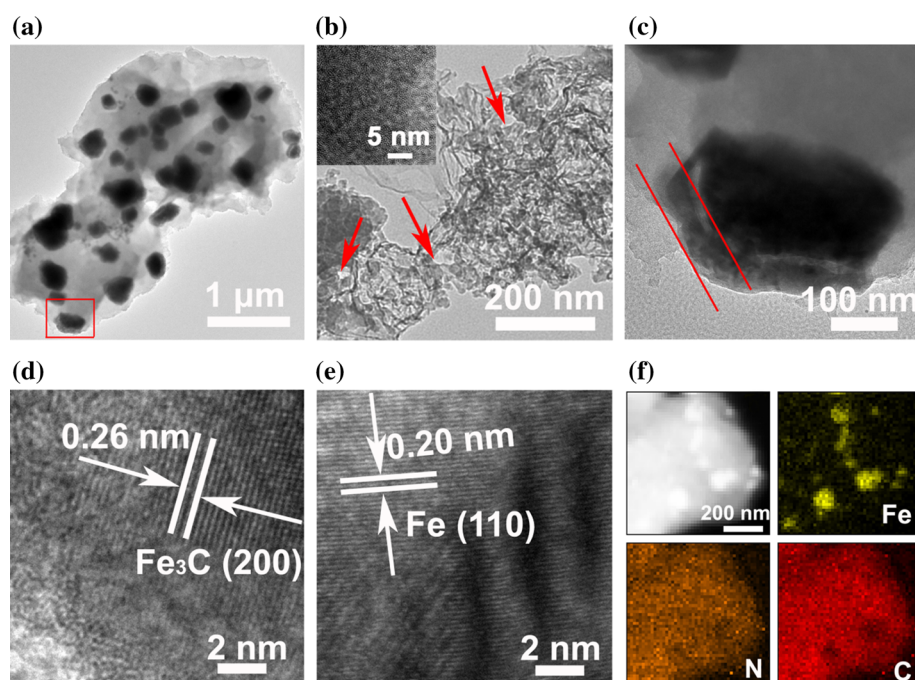
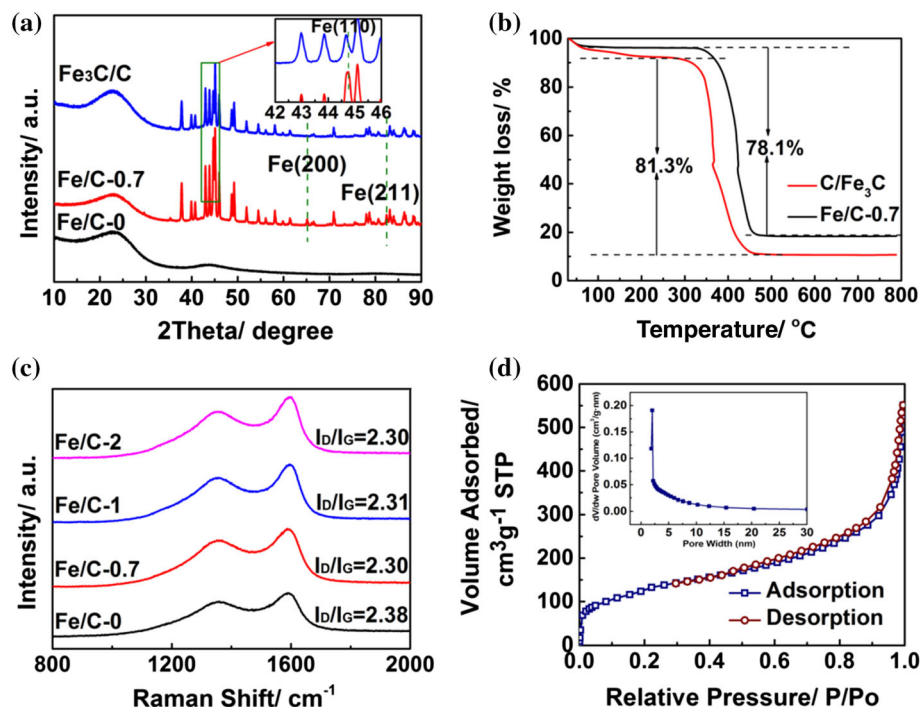


Figure 3 XRD patterns of Fe/Fe₃C/C and Fe₃C/C (the inset is the local magnification of the rectangle) (a), TG curves of Fe/Fe₃C/C and Fe₃C/C (b), Raman spectra of Fe/C composites (c), nitrogen adsorption–desorption isotherms (the inset is the pore-size distributions) (d).



82.3° are assigned to the (110), (200) and (211) planes of α -Fe (JCPDS No. 65-4889), respectively. The XRD result of Fe/C-0.7 is in accordance with those of HRTEM. The disappearance of the Fe₂O₃ diffraction peaks suggests that it has been completely transformed. The formation of Fe₃C is due to reaction between reductive iron and carbon matrix at 650 °C. According to the Rietveld refinement, the relative contents of Fe and Fe₃C in the crystalline phase for Fe/C-0.7 are 13.4 wt% and 86.6 wt%, respectively. For Fe/C-1 and Fe/C-2, the diffraction intensities of iron become stronger (see Fig. S5), and the relative contents of metal Fe in the crystalline phase are deduced as 44.2 wt% and 73.1 wt%, respectively. Because the stability of Fe₃C is higher than that of iron, the iron in the composites can be removed by 30 wt% tartaric acid to obtain Fe₃C/C [45]. Diffraction peaks are not observed for iron in the XRD pattern of the Fe₃C/C sample, and the main peak of iron located at 44.6° disappears at the local magnification of XRD, which is inserted in Fig. 3a, indicating the thorough removal of iron in the composites. The XRD results demonstrate that the mass ratio of Fe to Fe₃C in the composites can be modified by the proportion of raw materials. To further analyze the composition of the composites, TG tests of samples Fe/C-0.7 and Fe₃C/C are carried out in air (Fig. 3b). Fe/C-0.7 and Fe₃C/C have total weight

losses of 78.1 wt% and 81.3 wt%, respectively, corresponding to the carbon contents in the composites. According to the difference values of weight loss in composites, the Fe and Fe₃C contents are estimated to be approximately 3.2 wt% and 18.7% in Fe/C-0.7, respectively. The mass ratio of Fe to Fe₃C determined by TG is very close to that calculated by XRD refinement. To analyze the microstructure of the carbon, Raman tests are carried out. As shown in the Raman spectra (Fig. 3c), both carbon spheres (Fe/C-0) and Fe/C composites exhibit two distinguishable peaks attributed to D-bands (1350 cm⁻¹) and G-bands (1595 cm⁻¹). More interestingly, the ratios of D-bands and G-bands (I_D/I_G) for the Fe/C composites (Fe/C-0.7, Fe/C-1 and Fe/C-2) are almost identical and are slightly higher than that of Fe/C-0 due to the catalysis of iron [46, 47]. The value for I_D/I_G is higher than that of N-doped graphene [48], indicating incomplete graphitization with short-range order, which agrees with the results of the HRTEM images and XRD. Nitrogen adsorption–desorption analysis is utilized to further analyze the structural information of the Fe/C composites. As observed in Fig. 3d, sample Fe/C-0.7 presents a long and narrow loop at a relative pressure (P/P_0) between 0.3 and 1.0, corresponding to the IV-type isotherm adsorption curve in terms of IUPAC classification, which is a distinctive characteristic of mesoporous materials [49]. The BET

surface area and BJH pore size distribution of Fe/C-0.7 are $451.7 \text{ m}^2 \text{ g}^{-1}$ and 2.16 nm (see insert of Fig. 3d), respectively, conforming with the conclusion of a mesoporous structure. Compared with the most porous carbon [50], the synthesized porous carbon has a lower BET surface area.

The surface chemical composition is analyzed by XPS. The XPS survey of Fe/C-0.7 (Fig. 4a) demonstrates binding energy peaks at 285, 400, 530 and 711 eV associated with C1s, N1s, O1s and Fe2p, respectively. To further analyze the binding bonds of the elements, high-resolution XPS spectra of Fe and N are analyzed in Fig. 4b and c, respectively. As shown, the spin-orbit Fe 2p_{1/2} and Fe 2p_{3/2} appear at 725.2 eV and 711.3 eV, respectively, corresponding to Fe₃C [51]. Pure Fe and iron oxides cannot be detected by XPS, suggesting that the surface Fe is only present as Fe₃C. Moreover, the atomic ratio of Fe is only 1.43% in Fe/C-0.7 XPS, which is distinctly lower than that of the XRD and TG results. As discussed above, the Fe₂O₃ nanoparticles are embedded in the APF matrix. Therefore, the reduced Fe particles are still embedded in the carbon matrix. Fe₃C forms when iron particles react with carbon. A part of the Fe₃C is exposed at the surface under carbonization of APF. Therefore, Fe₃C is the only possible component containing Fe exposed on the surface of composites, which guarantees the stability of the composites. In

addition, the XPS can only analyze surface element binding energy in several nanometers depth of samples. Therefore, XPS can only detect Fe₃C in Fe/C-0.7. As seen in Fig. 4c, the peaks at 398.6 and 400.9 eV are assigned from N1s, which are associated with pyridine nitrogen and graphitic nitrogen, indicating the N-doping of carbon [48, 52]. The XPS survey (Fig. 4d), Fe 2p (Fig. 4e), and N 1s (Fig. 4f) spectra of Fe₃C/C show results similar to those of Fe/C-0.7(Fe/Fe₃C/C). In addition, the atomic ratio of Fe in the XPS results for Fe₃C/C is 1.66%, which is close to that of Fe/Fe₃C/C. The XPS results for Fe₃C/C further confirm that the existence of Fe element on the surface of the synthesized Fe/C composites is only present as Fe₃C.

The room-temperature magnetic hysteresis loops of N-doped carbon embedded with Fe/Fe₃C particles are shown in Fig. S6. The saturation magnetization (M_s) of samples Fe/C-0, Fe/C-0.7, Fe/C-1 and Fe/C-2 are 0.17 emu/g, 13.26 emu/g, 15.06 emu/g and 20.12 emu/g, respectively. The Fe/C composites show low saturation magnetization due to the small amount of iron in the composites. The decreasing tendency of the magnetization values from Fe/C-2 to Fe/C-0.7 mainly results from the reduction of in the mass ratio of iron in the composites (as shown in the XRD refinement).

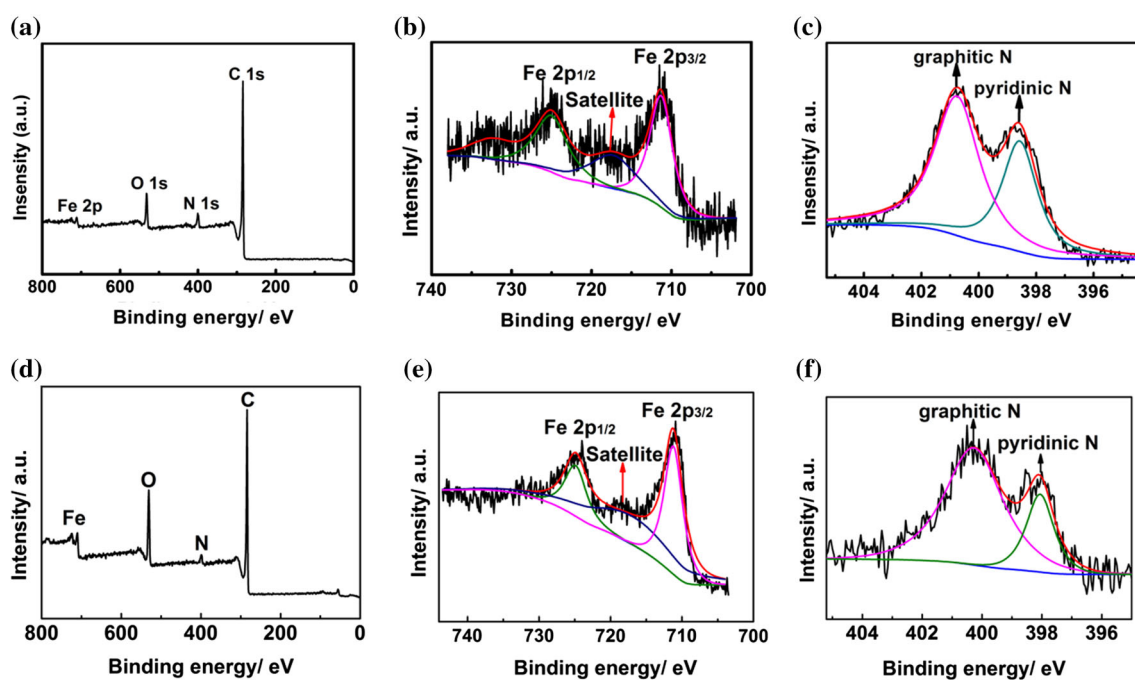
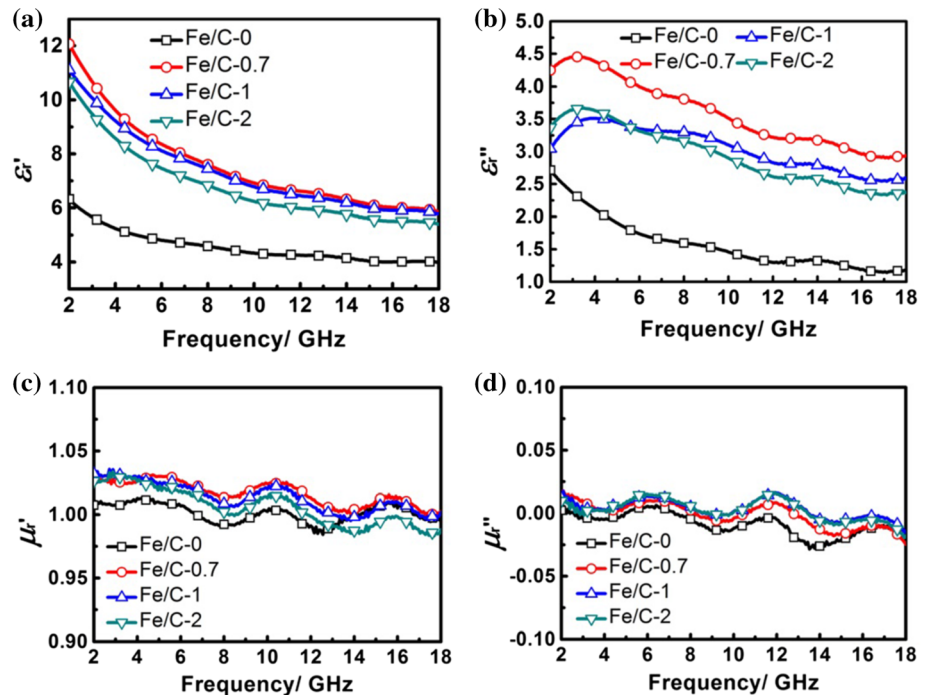


Figure 4 XPS survey (a), Fe 2p (b), N 1s (c) spectra of Fe/Fe₃C/C and XPS survey (d), Fe 2p (e), N 1s (f) spectra of Fe₃C/C.

Figure 5 Frequency dependence of the real (a) and imaginary (b) parts of the relative complex permittivity and the real (c) and imaginary (d) parts of the relative complex permeability for the Fe/C composites.



The frequency dependence of the electromagnetic parameters for the carbon spheres and N-doped carbon embedded with Fe/Fe₃C particles is shown in Fig. 5. As displayed in Fig. 5a and b, the ϵ_r values of all the Fe/C samples show frequency dependence over the frequency range of 2.0–18.0 GHz. The ϵ_r' and ϵ_r'' values of the pure N-doped carbon spheres (sample Fe/C-0) decrease from 6.3 to 4.0 and 2.7 to 1.8 in the measured frequency range, respectively. For the N-doped carbon with embedded Fe/Fe₃C particles, both the ϵ_r' and ϵ_r'' values are evidently enhanced. In detail, ϵ_r' values of Fe/C-0.7, Fe/C-1 and Fe/C-2 gradually decrease from 12.0, 11.1, 10.7 at 2.0 GHz to 5.9, 5.8, and 5.4 at 18.0 GHz, respectively. The corresponding ϵ_r'' values increase from 4.2, 3.0, and 3.4 at 2.0 GHz to 4.5, 3.5, and 3.7 at 3.2 GHz and then decrease to 3.0, 2.6, and 2.4 at 18.0 GHz, respectively. It is worth noting that the N-doped carbon with embedded Fe/Fe₃C particles and carbon spheres exhibits frequency dispersion, which is beneficial for improving the microwave absorption ability [53, 54]. According to the free-electron theory, both Fe and C have certain electrical conductivities. Therefore, the microwave energy can be diminished by conductive loss in Fe and carbon composites. However, it is difficult to form a conductive network because the Fe particles dispersed in the porous turbostratic carbon matrix are coated by a Fe₃C shell, resulting in a low

electric conductivity. Although the conductive loss of the composites is limited, the modest conductivity not only favors the consumption of electromagnetic energy but also guarantees good impedance matching, ensuring the entrance of electromagnetic wave into the composites [5]. In addition, polarization relaxation is another very important factor influencing the dielectric loss of the composites. Compared with the carbon spheres, the ϵ_r'' curves of the N-doped carbon with embedded Fe/Fe₃C display fluctuations, which is usually related to the attenuation of electromagnetic wave via polarization relaxation [55, 56]. As demonstrated by the results of Raman, XRD and TEM, the graphitization degree of nitrogen doped carbon is adjusted through the addition of iron. It is worth noting that the carbon presents a turbostratic structure with short range-order, which generates microcurrent in the short range-order carbon under electromagnetic wave. On the one hand, nitrogen doping in carbon can produce abundant defects that could serve as the dipole center and produce dipole polarization relaxation, enhancing the dielectric loss ability of the composites [27, 57]. On the other hand, the difference between the conductivities of Fe, Fe₃C and turbostratic carbon lead to the accumulation of a large amount of charge at the interface, resulting in multiple interfacial polarization relaxations when exposed to the electromagnetic field. Therefore,

compared with the pure N-doped carbon spheres, the composites of N-doped carbon with embedded Fe/Fe₃C possess higher permittivity because there are multiple interfacial polarizations between the Fe/Fe₃C particles and N-doped carbon. The interfacial polarization is affected by the mass ratio of Fe to Fe₃C. To further reveal the effect of interfacial polarization on the dielectric loss, the electromagnetic properties of Fe₃C/C with the same microstructure of Fe/Fe₃C/C are studied. As expected, the ϵ_r' values of Fe₃C/C are lower than those of Fe/Fe₃C/C due to the removal of iron (Fig. S7a). The ϵ_r'' values of Fe₃C/C are also lower than that of Fe/Fe₃C/C in most frequency ranges as a result of the disappearance of the interface between Fe and Fe₃C (Fig. S7a). In general, multiple interfacial polarization relaxation plays a critical role in determining the dielectric loss properties in the N-doped carbon with embedded Fe/Fe₃C composites. Moreover, porous structure in N-doped carbon provides more opportunity for contact between the microwave and absorber, leading to multiple reflection and scattering, which further improve the attenuation property of the composites [58, 59].

As shown in Fig. 5c and d, the values of the real (μ_r') and imaginary parts (μ_r'') of the relative complex permeability of N-doped carbon spheres are close to 1 and 0, respectively, which corresponds to the typical characteristics of nonmagnetic materials. The values of μ_r' and μ_r'' of samples Fe/C-0.7, Fe/C-1 and Fe/C-2 are similar and are maintained at approximately 1.02 and 0.02, respectively, with several small fluctuations over the whole frequency range. Although the magnetic properties in Fe/C-0.7, Fe/C-1, and Fe/C-2 are different, which is determined by VSM, the magnetic loss of the composites is very close, expressed by the similar μ_r' and μ_r'' . The values of μ_r'' of the N-doped carbon with embedded Fe/Fe₃C composites are close to 0 over most of the investigated frequency range, which is much lower than that of iron particles [60, 61], revealing that the magnetic loss is very limited. The low content of iron and Fe₃C in the composites is the main cause of the low magnetic loss. The frequency dependences of the μ_r' and μ_r'' values of Fe₃C/C are similar to those of Fe/Fe₃C/C (Fig. S7b), further confirming the small effect of magnetic components on magnetic loss in Fe/Fe₃C/C composites. In view of the above analysis, the enhancement of the attenuation capacity of N-doped

carbon with embedded Fe/Fe₃C composites mainly originates from dielectric loss, especially multiple interfacial polarizations. The small contents of iron and Fe₃C do not obviously generate magnetic loss. However, the presence of iron nanoparticles has a crucial catalytic effect on the carbonization of aminophenol formaldehyde resin, affecting the intense dipole polarization in the carbon matrix. Furthermore, the Fe/Fe₃C particles in the composites play a critical role in interfacial polarization.

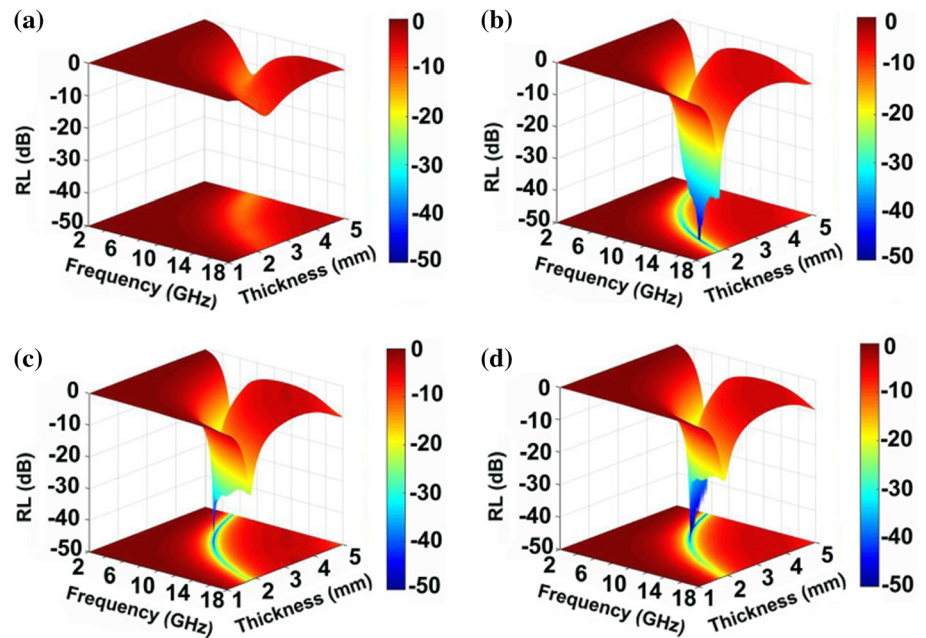
In general, the microwave absorption performance of absorbers can be assessed through transmission line theory [4, 62]:

$$RL(\text{dB}) = 20 \log |(Z_{\text{in}} - 1)/(Z_{\text{in}} + 1)| \tag{1}$$

$$Z_{\text{in}} = \sqrt{\frac{\mu_r}{\epsilon_r}} \tanh \left[j \left(\frac{2\pi f d}{c} \right) \sqrt{\mu_r \epsilon_r} \right] \tag{2}$$

The microwave absorption (MA) performances of Fe/C-0, Fe/C-0.7, Fe/C-1, Fe/C-2 and Fe₃C/C with thicknesses of 1.0–5.0 mm over the frequency range of 2.0–18.0 GHz are presented in Fig. 6 and Fig. S7c, respectively. As detected, the MA performances of the as-prepared composites are greatly influenced by the addition of iron. The minimum value of reflection loss for N-doped carbon sphere-sample Fe/C-0 is – 13 dB at 7.44 GHz with a thickness of 5.00 mm (Fig. 6a). The Fe/Fe₃C particles embedded in the N-doped net-like carbon matrix may boost the MA performance, and the minimum values for Fe/C-0.7, Fe/C-1, Fe/C-2 and Fe₃C/C are – 57 dB (14.56 GHz), – 50 dB (7.92 GHz), – 70 dB (7.52 GHz) and – 53 dB (9.84 GHz) at matching thicknesses of 2.13 mm, 3.55 mm, 3.88 mm, and 3.49 mm, respectively. For the purpose of comparison, the RL in Fig. 6 end at – 50.0 dB. Additionally, the RL curves corresponding to the minimum values at matching thickness are shown in Fig. S8a. The strong absorption intensity is one key factor for microwave absorption materials. In addition, broadband response is another important characteristic of highly efficient microwave absorption materials in actual applications. The effective absorption bandwidths of Fe/C-0, Fe/C-0.7, Fe/C-1, Fe/C-2 and Fe₃C/C are 2.09 GHz, 6.02 GHz, 3.20 GHz, 3.18 GHz and 4.40 GHz at the corresponding matching thicknesses, respectively. When the thickness is designated at 2.0 mm (Fig. S8b), the effective bandwidths of Fe/C-0, Fe/C-0.7, Fe/C-1, Fe/C-2 and Fe₃C/C are 0 GHz, 5.2 GHz (12.8–18.0 GHz), 4.6 GHz

Figure 6 Three-dimensional reflection loss (RL) maps of samples Fe/C-0 (a), Fe/C-0.7 (b), Fe/C-1 (c), and Fe/C-2 (d) with thicknesses of 1.0–5.0 mm.



(13.4–18.0 GHz), 3.8 GHz (14.2–18.0 GHz), and 2.2 GHz (15.8–18.0 GHz), respectively. The integrated effective absorption bandwidths (RL ≤ -10 dB) from 1.0 to 5.0 mm of Fe/C-0, Fe/C-0.7, Fe/C-1 and Fe/C-2 are 8.48 GHz (6.56–15.04 GHz), 13.68 GHz (4.32–18.0 GHz), 13.52 (4.48–18.0 GHz) and 13.36 GHz (4.64–18.0 GHz), respectively. Based on the above data, Fe/C-0.7, which contains the lowest amount of Fe, is the optimal candidate among these N-doped carbon Fe/Fe₃C particle embedded samples. Therefore, the molar ratio of Fe³⁺ to 3-AP is reduced to 0.5:1; unfortunately, the net-like structure embedded with nanoparticles cannot be obtained, as revealed in the TEM images (Fig. S9).

To estimate the superior attenuation ability of Fe/C-0.7, the total attenuation constants (α) are calculated via the following equation [48, 56]:

$$\alpha = \frac{\sqrt{2}\pi f}{c} \times \sqrt{(\mu_r \varepsilon_r - \mu_r' \varepsilon_r') + \sqrt{(\mu_r \varepsilon_r - \mu_r' \varepsilon_r')^2 + (\mu_r' \varepsilon_r + \mu_r \varepsilon_r')^2}} \quad (3)$$

As shown in Fig. 7a, the composites of N-doped carbon with embedded Fe/Fe₃C particles exhibit larger value of α than that of carbon spheres (Fe/C-0), and Fe/C-0.7 shows the maximum value among the composites, confirming its superior attenuation ability. To determine the origin of the attenuation, the dielectric loss factor ($\tan \delta_e = \varepsilon_r'' / \varepsilon_r'$) and magnetic loss factor ($\tan \delta_m = \mu_r'' / \mu_r'$) of the composites are exhibited in Fig. 7b and c, respectively. As shown, the dielectric loss factor of N-doped carbon with embedded Fe/Fe₃C particles is distinctly higher than that of the carbon spheres in the frequency range of

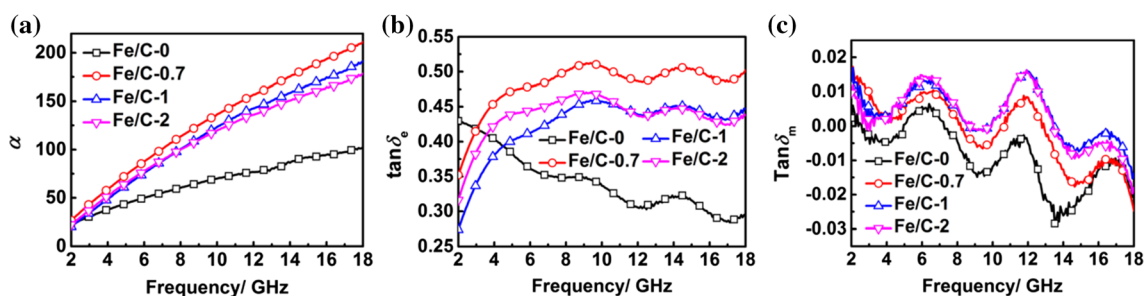


Figure 7 Total attenuation constants α (a), dielectric loss factor $\tan \delta_e$ (b), and magnetic loss factor $\tan \delta_m$ (c) of samples Fe/C-0, Fe/C-0.7, Fe/C-1, Fe/C-2.

4.2–18.0 GHz, which indicates the superior dielectric loss of the composites. Although the magnetic loss is limited over the frequency of 2.0–4.2 GHz, as discussed above, the magnetic loss factor of the composites is higher than that of the carbon spheres. Therefore, over 2.0–4.2 GHz, the magnetic loss is another important way for the total attenuation of the composites. Overall, the dielectric loss factor of Fe/C-0.7 is the highest among the composites over the frequency of 3.0–18.0 GHz. Hence, the superior attenuation ability of Fe/C-0.7 is mainly caused by the dielectric loss ascribed to multiple interfacial polarization relaxations and scattering of microwave in the N-doped carbon with an appropriate content of embedded Fe/Fe₃C particles, resulting in good MA performance.

The mechanisms of enhanced microwave attenuation in N-doped carbon with embedded Fe/Fe₃C

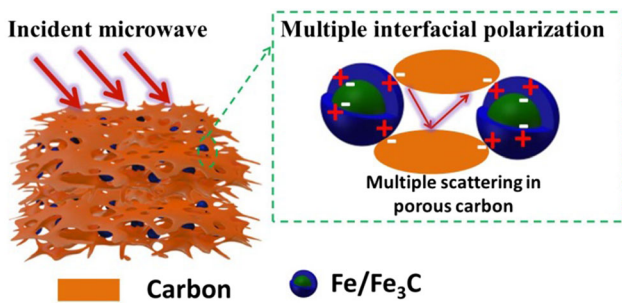


Figure 8 Schematic illustration of interfacial polarization and scattering in N-doped carbon with embedded Fe/Fe₃C particles.

particles are illustrated in Fig. 8, which schematically shows multiple interfacial polarizations, multiple reflection and scattering in porous composite. The interfacial polarization associated with the interface between Fe₃C–Fe, Fe₃C–C and carbon holes in the composites is caused by their different conductivities when irradiated under electromagnetic wave. In addition, the porous structure of the N-doped carbon embedded with Fe/Fe₃C can lead to a geometric effect for multiple reflection and scattering, providing more opportunities for the attenuation of incident microwaves. Compared with pure N-doped carbon spheres and Fe₃C/C, the Fe/Fe₃C/C composites indicate excellent MA performance determined by the composition, morphology, and microstructure that ultimately dictate the interfacial polarization in the composite.

Table 1 displays a comparison of the strongest microwave absorption, matching thickness and effective bandwidth of Fe/C-0.7 with those of similar composites in recent references, emphasizing the prospective application of Fe/C-0.7 as an MAM with excellent performance. The improvement in the electromagnetic wave absorption for the synthesized composites is mainly due to the unique microstructure and components obtained from the heat treatment on the precursor of APF/Fe₂O₃ with a net-like structure. Due to the nitrogen atom doping in the carbon matrix, there are many defects in the carbon, which is beneficial to the dipole polarization in the composite. In addition, the interface polarization is

Table 1 Comparison of microwave absorption of the various carbon and iron composites

Materials	Maximum RL (dB)	Effective bandwidth (RL ≤ - 10 dB, GHz)	Corresponding thickness (mm)	Effective bandwidth (2.0 mm, GHz)	Ref.
Porous 3D Fe/C composites	- 58	5.3	3.95	< 4.0	[48]
Fe/Fe ₃ C@NCNTs	- 46	1.0	4.97	3.0	[56]
Fe–C nanofiber	- 44	–	–	2.0	[57]
3D cross-linked Fe/C porous nanofibers	- 57	1.8	4.29	3.0	[63]
C/Fe ₃ C nanocomposites	- 41	3.0	3.50	5.6	[55]
Fe–Fe ₃ C/C microspheres	- 18	4.0	1.50	2.8	[64]
Centipede-shaped Fe/Fe ₃ C/MWCNT	- 32	2.6	2.00	2.6	[65]
Fe/Fe ₃ C/C core–shell spherical chains	- 58	2.1	2.40	3.0	[66]
Core–shell Fe-Fe ₃ C@C	- 18	3.4	2.00	3.4	[67]
Porous N-doped carbon embedded Fe/Fe ₃ C	- 57	6.0	2.13	5.2	Our work

promoted due to the existence of a large number of contact interfaces between different components with different conductivities. In particular, the enhanced microwave absorption performance of Fe/C-0.7 should be ascribed to the intense dielectric loss caused by multiple interfacial polarizations between Fe/Fe₃C and N-doped carbon, which produces enhanced dielectric loss and attenuation ability.

Conclusion

N-doped carbon with embedded Fe/Fe₃C particles is synthesized in-situ through pyrolysis of amino-phenol formaldehyde resin (APF) scattered with Fe₂O₃ nanoparticles (APF/Fe₂O₃), which was obtained through a simple hydrothermal process. The as-synthesized composites present high-efficient microwave absorption with an effective absorption bandwidth of 6.02 GHz at a thickness of only 2.13 mm. The microwave absorption of the as-synthesized composites mainly comes from the multiple interfacial polarization occurring between the different mediums. This study indicates that N-doped carbon with embedded Fe/Fe₃C particles is a promising high-efficient MAM.

Acknowledgements

This work was supported by National Natural Science Foundation of China (Grant No. 51802278), Natural Science Foundation of Hebei Province (Grant No. E2018203274), and China Postdoctoral Science Foundation (Grant No. 2017M621102).

Compliance with ethical standards

Conflict of interest The authors declare there is no conflict of interest.

Electronic supplementary material: The online version of this article (<https://doi.org/10.1007/s10853-020-04918-7>) contains supplementary material, which is available to authorized users.

References

- [1] Shahzad F, Alhabeab M, Hatter CB, Anasori B, Hong SM, Koo CM, Gogotsi Y (2016) Electromagnetic interference shielding with 2D transition metal carbides (MXenes). *Science* 353:1137–1140
- [2] Wang Q-W, Zhang H-B, Liu J, Zhao S, Xie X, Liu L, Yang R, Koratkar N, Yu Z-Z (2019) Multifunctional and water-resistant MXene-decorated polyester textiles with outstanding electromagnetic interference shielding and Joule heating performances. *Adv Funct Mater* 29:1806819
- [3] Liu Q, Cao Q, Bi H, Liang C, Yuan K, She W, Yang Y, Che R (2016) CoNi@SiO₂@TiO₂ and CoNi@Air@TiO₂ microspheres with strong wideband microwave absorption. *Adv Mater* 28:486–490
- [4] Zhou C, Wu C, Yan M (2019) A versatile strategy towards magnetic/dielectric porous heterostructure with confinement effect for lightweight and broadband electromagnetic wave absorption. *Chem Eng J* 370:988–996
- [5] Qiang R, Du Y, Zhao H, Wang Y, Tian C, Li Z, Han X, Xu P (2015) Metal organic framework-derived Fe/C nanocubes toward efficient microwave absorption. *J Mater Chem A* 3:13426–13434
- [6] Zhang L, Zhang X, Zhang G, Zhang Z, Liu S, Li P, Liao Q, Zhao Y, Zhang Y (2015) Investigation on the optimization, design and microwave absorption properties of reduced graphene oxide/tetrapod-like ZnO composites. *RSC Adv* 5:10197–10203
- [7] Li X, Du D, Wang C, Wang H, Xu Z (2018) In situ synthesis of hierarchical rose-like porous Fe@C with enhanced electromagnetic wave absorption. *J Mater Chem C* 6:558–567
- [8] Shen G, Ren J, Zhao B, Mei B, Wu H, Fang X, Xu Y (2019) Magnetic hollow mesoporous carbon composites with impedance matching for highly effective microwave absorption. *J Mater Sci* 54:4024–4037. <https://doi.org/10.1007/s10853-018-3100-z>
- [9] Ding Y, Zhang Z, Luo B, Liao Q, Liu S, Liu Y, Zhang Y (2017) Investigation on the broadband electromagnetic wave absorption properties and mechanism of Co₃O₄-nanosheets/reduced-graphene-oxide composite. *Nano Res* 10:980–990
- [10] Wang X, Huang X, Chen Z, Liao X, Liu C, Shi B (2015) Ferromagnetic hierarchical carbon nanofiber bundles derived from natural collagen fibers: truly lightweight and high-performance microwave absorption materials. *J Mater Chem C* 3:10146–10153
- [11] Li G, Xie T, Yang S, Jin J, Jiang J (2012) Microwave absorption enhancement of porous carbon fibers compared with carbon nanofibers. *J Phys Chem C* 116:9196–9201
- [12] Sun H, Che R, You X, Jiang Y, Yang Z, Deng J, Qiu L, Peng H (2014) Cross-stacking aligned carbon-nanotube films to tune microwave absorption frequencies and increase absorption intensities. *Adv Mater* 26:8120–8125
- [13] Hu C, Liu H, Zhang Y, Zhang M, Yu J, Liu X, Zhang X (2019) Tuning microwave absorption properties of

- multiwalled carbon nanotubes by surface functional groups. *J Mater Sci* 54:2417–2426. <https://doi.org/10.1007/s10853-018-2895-y>
- [14] Kuang B, Song W, Ning M, Li J, Zhao Z, Guo D, Cao M, Jin H (2018) Chemical reduction dependent dielectric properties and dielectric loss mechanism of reduced graphene oxide. *Carbon* 127:209–217
- [15] Zhang Y, Huang Y, Chen H, Huang Z, Yang Y, Xiao P, Zhou Y, Chen Y (2016) Composition and structure control of ultralight graphene foam for high-performance microwave absorption. *Carbon* 105:438–447
- [16] Cao M, Han C, Wang X, Zhang M, Zhang Y, Shu J, Yang H, Fang X, Yuan J (2018) Graphene nanohybrids: excellent electromagnetic properties for the absorbing and shielding of electromagnetic waves. *J Mater Chem C* 6:4586–4602
- [17] Cheng Y, Li Z, Li Y, Dai S, Ji G, Zhao H, Cao J, Du Y (2018) Rationally regulating complex dielectric parameters of mesoporous carbon hollow spheres to carry out efficient microwave absorption. *Carbon* 127:643–652
- [18] Xu H, Yin X, Zhu M, Han M, Hou Z, Li X, Zhang L, Cheng L (2017) Carbon hollow microspheres with a designable mesoporous shell for high-performance electromagnetic wave absorption. *ACS Appl Mater Interfaces* 9:6332–6341
- [19] Qiu X, Wang L, Zhu H, Guana Y, Zhang Q (2017) Lightweight and efficient microwave absorbing materials based on walnut shell-derived nanoporous carbon. *Nanoscale* 9:7408–7418
- [20] Li Q, Zhang Z, Qi L, Liao Q, Kang Z, Zhang Y (2019) Toward the application of high frequency electromagnetic wave absorption by carbon nanostructures. *Adv Sci* 6:1801057
- [21] Qiang R, Du Y, Wang Y, Wang N, Tian C, Ma J, Xu P, Han X (2016) Rational design of yolk-shell C@C microspheres for the effective enhancement in microwave absorption. *Carbon* 98:599–606
- [22] Chu W, Wang Y, Du Y, Qiang R, Tian C, Han X (2017) FeCo alloy nanoparticles supported on ordered mesoporous carbon for enhanced microwave absorption. *J Mater Sci* 52:13636–13649. <https://doi.org/10.1007/s10853-017-1439-1>
- [23] Zhang Y, Huang Y, Zhang T, Chang H, Xiao P, Chen H, Huang Z, Chen Y (2015) Broadband and tunable high-performance microwave absorption of an ultralight and highly compressible graphene foam. *Adv Mater* 27:2049–2053
- [24] Li S, Huang Y, Ling D, Zhang N, Zong M, Qin X, Liu P (2019) Enhanced microwave-absorption with carbon-encapsulated Fe-Co particles on reduced graphene oxide nanosheets with nanoscale-holes in the basal plane. *J Coll Interface Sci* 544:188–197
- [25] Li Y, Zhou Z, Shen P, Chen Z (2009) Spin gapless semiconductor-metal-half-metal properties in nitrogen-doped zigzag graphene nanoribbons. *ACS Nano* 3:1952–1958
- [26] Shin WH, Jeong HM, Kim BG, Kang JK, Choi JW (2012) Nitrogen-doped multiwall carbon nanotubes for lithium storage with extremely high capacity. *Nano Lett* 12:2283–2288
- [27] Liu P, Zhang Y, Yan J, Huang Y, Xia L, Guang Z (2019) Synthesis of lightweight N-doped graphene foams with open reticular structure for high-efficiency electromagnetic wave absorption. *Chem Eng J* 368:285–298
- [28] Ouyang J, Liu T, Yang H, Zhang Y (2019) Multiple polarization loss and permittivity adjusting of halloysite/BN Co-doped carbon/cobalt composites. *J Coll Interface Sci* 555:509–518
- [29] Li H, Bao S, Li Y, Huang Y, Chen J, Zhao H, Jiang Z, Kuang Q, Xie Z (2018) Optimizing the electromagnetic wave absorption performances of designed $\text{Co}_3\text{Fe}_7\text{@C}$ yolk-shell structures. *ACS Appl Mater Interfaces* 10:28839–28849
- [30] Jian X, Xiao X, Deng L, Tian W, Wang X, Mahmood N, Dou S (2018) Heterostructured nanorings of $\text{Fe}-\text{Fe}_3\text{O}_4\text{@C}$ hybrid with enhanced microwave absorption performance. *ACS Appl Mater Interfaces* 10:9369–9378
- [31] Ding Y, Zhang L, Liao Q, Zhang G, Liu S, Zhang Y (2016) Electromagnetic wave absorption in reduced graphene oxide functionalized with $\text{Fe}_3\text{O}_4/\text{Fe}$ nanorings. *Nano Res* 9:2018–2025
- [32] Fang J, Liu T, Chen Z, Wang Y, Wei W, Yue X, Jiang Z (2016) A wormhole-like porous carbon/magnetic particles composite as an efficient broadband electromagnetic wave absorber. *Nanoscale* 8:8899–8909
- [33] Lü Y, Wang Y, Li H, Lin Y, Jiang Z, Xie Z, Kuang Q, Zheng L (2015) MOF-derived porous Co/C nanocomposites with excellent electromagnetic wave absorption properties. *ACS Appl Mater Interfaces* 7:13604–13611
- [34] Zhang X, Ji G, Liu W, Quan B, Liang X, Shang C, Cheng Y, Du Y (2015) Thermal conversion of an $\text{Fe}_3\text{O}_4\text{@metal-organic framework}$: a new method for an efficient Fe-Co/nanoporous carbon microwave absorbing material. *Nanoscale* 7:12932–12942
- [35] Zhao H, Cheng Y, Lv H, Zhang B, Ji G, Du Y (2018) Achieving sustainable ultralight electromagnetic absorber from flour by turning surface morphology of nanoporous carbon. *ACS Sustain Chem Eng* 6:15850–15857
- [36] Liu Q, Liu X, Feng H, Shui H, Yu R (2017) Metal organic framework-derived Fe/carbon porous composite with low Fe content for lightweight and highly efficient electromagnetic wave absorber. *Chem Eng J* 314:320–327
- [37] Shu R, Li W, Wu Y, Zhang J, Zhang G (2019) Nitrogen-doped Co-C/MWCNTs nanocomposites derived from

- bimetallic metal–organic frameworks for electromagnetic wave absorption in the X-band. *Chem Eng J* 362:513–524
- [38] Tang J, Wang T, Pan X, Sun X, Fan X, Guo Y, Xue H, He J (2013) Synthesis and electrochemical characterization of N-doped partially graphitized ordered mesoporous carbon–Co composite. *J Phys Chem C* 117:16896–16906
- [39] Zhang X, Yan F, Zhang S, Yuan H, Zhu C, Zhang X, Chen Y (2018) Hollow N-doped carbon polyhedron containing CoNi alloy nanoparticles embedded within few-layer N-doped graphene as high-performance electromagnetic wave absorbing material. *ACS Appl Mater Interfaces* 10:24920–24929
- [40] Qiao M, Lei X, Ma Y, Tian L, He X, Su K, Zhang Q (2018) Application of yolk–shell Fe_3O_4 @N-doped carbon nanochains as highly effective microwave-absorption material. *Nano Res* 11:1500–1519
- [41] Li Z, Li X, Zong Y, Tan G, Sun Y, Lan Y, He M, Ren Z, Zheng X (2017) Solvothermal synthesis of nitrogen-doped graphene decorated by superparamagnetic Fe_3O_4 nanoparticles and their applications as enhanced synergistic microwave absorbers. *Carbon* 115:493–502
- [42] Liu H, Li Y, Yuan M, Sun G, Li H, Ma S, Liao Q, Zhang Y (2018) In situ preparation of cobalt nanoparticles decorated in n-doped carbon nanofibers as excellent electromagnetic wave absorbers. *ACS Appl Mater Interfaces* 10:22591–22601
- [43] Yuan H, Yan F, Li C, Zhu C, Zhang X, Chen Y (2018) Nickel nanoparticle encapsulated in few-layer nitrogen-doped graphene supported by nitrogen-doped graphite sheets as a high-performance electromagnetic wave absorbing material. *ACS Appl Mater Interfaces* 10:1399–1407
- [44] Wollbrink A, Volgmann K, Koch J, Kanthasamy K, Tegenkamp C, Li Y, Richter H, Kämnitz S, Steinbach F, Feldhoff A, Caro J (2016) Amorphous, turbostratic and crystalline carbon membranes with hydrogen selectivity. *Carbon* 106:93–105
- [45] Feng W, Liu M, Liu J, Song Y, Wang F (2018) Well-defined Fe, Fe_3C , and Fe_2O_3 heterostructures on carbon black: a synergistic catalyst for oxygen reduction reaction. *Catal Sci Technol* 8:4900–4906
- [46] Casco ME, Kirchhoff S, Leistenschneider D, Rauche M, Brunner E, Borchardt L (2019) Mechanochemical synthesis of N-doped porous carbon at room temperature. *Nanoscale* 11:4712–4718
- [47] Mutuma BK, Garcia-Martinez CI, Dias RC, Matsoso BJ, Coville NJ, Hümmelgen IA (2019) Nitrogen-doped hollow carbon spheres as chemical vapour sensors. *New J Chem* 43:8418–8427
- [48] Li X, Wang H, Robinson JT, Sanchez H, Diankov G, Dai H (2009) Simultaneous nitrogen doped and reduction of graphene oxide. *J Am Chem Soc* 131:15939–15944
- [49] Li C, Ji S, Jiang X, Waterhouse GIN, Zhang Z, Yu L (2018) Microwave absorption by watermelon-like microspheres composed of $\gamma\text{-Fe}_2\text{O}_3$, microporous silica and polypyrrole. *J Mater Sci* 53:9635–9649. <https://doi.org/10.1007/s10853-018-2262-z>
- [50] Puthiaraj P, Lee Y-R, Ahn W-S (2017) Microporous amine-functionalized aromatic polymers and their carbonized products for CO_2 adsorption. *Chem Eng J* 319:65–74
- [51] Lou Z, Li Y, Han H, Ma H, Wang L, Cai J, Yang L, Yuan C, Zou J (2018) Synthesis of porous 3D Fe/C composites from waste wood with tunable and excellent electromagnetic wave absorption performance. *ACS Sustain Chem Eng* 6:15598–15607
- [52] Jiang W-J, Gu L, Li L, Zhang Y, Zhang X, Zhang L-J, Wang J-Q, Hu J-S, Wei Z, Wan L-J (2016) Understanding the high activity of Fe–N–C electrocatalysts in oxygen reduction: Fe/ Fe_3C nanoparticles boost the activity of Fe–N $_x$. *J Am Chem Soc* 138:3570–3578
- [53] Chen Y-J, Xiao G, Wang T-S, Ouyang Q-Y, Qi L-H, Ma Y, Gao P, Zhu C-L, Cao M-S, Jin H-B (2011) Porous Fe_3O_4 /carbon Core/shell nanorods: synthesis and electromagnetic properties. *J Phys Chem C* 115:13603–13608
- [54] Wang Z, Wei R, Gu J, Liu H, Liu C, Luo C, Kong J, Shao Q, Wang N, Guo Z, Liu X (2018) Ultralight, highly compressible and fire-retardant graphene aerogel with self-adjustable electromagnetic wave absorption. *Carbon* 139:1126–1135
- [55] Zhang Y, Liu W, Quan B, Ji G, Ma J, Li D, Meng W (2017) Achieving the interfacial polarization on C/ Fe_3C heterojunction structures for highly efficient lightweight microwave absorption. *J Coll Interface Sci* 508:462–468
- [56] Xu Z, Du Y, Liu D, Wang Y, Ma W, Wang Y, Xu P, Han X (2019) Pea-like Fe/ Fe_3C nanoparticles embedded in nitrogen-doped carbon nanotubes with tunable dielectric/magnetic loss and efficient electromagnetic absorption. *ACS Appl Mater Interfaces* 11:4268–4277
- [57] Wang T, Wang H, Chi X, Li R, Wang J (2014) Synthesis and microwave absorption properties of Fe–C nanofibers by electrospinning with disperse Fe nanoparticles parceled by carbon. *Carbon* 74:312–318
- [58] Xu H, Yin X, Li M, Ye F, Han M, Hou Z, Li X, Zhang L, Cheng L (2018) Mesoporous carbon hollow microspheres with red blood cell like morphology for efficient microwave absorption at elevated temperature. *Carbon* 132:343–351
- [59] Cheng Y, Zhao H, Zhao Y, Cao J, Zheng J, Ji G (2020) Structure-switchable mesoporous carbon hollow sphere

- framework toward sensitive microwave response. *Carbon* 161:870–879
- [60] Li X, Qu X, Xu Z, Dong W, Wang F, Guo W, Wang H, Du Y (2019) Fabrication of three-dimensional flower-like heterogeneous Fe₃O₄/Fe particles with tunable chemical composition and microwave absorption performance. *ACS Appl Mater Interfaces* 11:19267–19276
- [61] Yu Z, Yao Z, Zhang N, Wang Z, Li C, Han X, Wu X, Jiang Z (2013) Electric field-induced synthesis of dendritic nanostructured α -Fe for electromagnetic absorption application. *J Mater Chem A* 1:4571–4576
- [62] Liu J, Cao MS, Luo Q, Shi H-L, Wang W-Z, Yuan J (2016) Electromagnetic property and tunable microwave absorption of 3D nets from nickel chains at elevated temperature. *ACS Appl Mater Interfaces* 8:22615–22622
- [63] Wang F, Sun Y, Li D, Zhong B, Wu Z, Zuo S, Yan D, Zhuo R, Feng J, Yan P (2018) Microwave absorption properties of 3D cross-linked Fe/C porous nanofibers prepared by electrospinning. *Carbon* 134:264–273
- [64] Li W, Qi H, Niu X, Guo F, Chen X, Wang L, Lv B (2016) Fe–Fe₃C/C microspheres as a lightweight microwave absorbent. *RSC Adv* 6:24820–24826
- [65] Tong G, Liu Y, Liu F, Guan J (2015) Easy gas-flow-induced CVD synthesis and tunable electromagnetic characteristics of centipede-shaped iron/cementite/multiwalled carbon nanotube (Fe/Fe₃C/MWCNT) heterostructures. *Surf Coat Technol* 283:286–297
- [66] Sun JC, He Z, Dong W, Wu W, Tong G (2019) Broadband and strong microwave absorption of Fe/Fe₃C/C core–shell spherical chains enhanced by dual dielectric relaxation and dual magnetic resonances. *J Alloy Compd* 782:193–202
- [67] Li G, Wang L, Li W, Xu Y (2015) Mesoporous Fe/C and core–shell Fe–Fe₃C@C composites as efficient microwave absorbents. *Microporous Mesoporous Mater* 211:97–104

Publisher's Note Springer Nature remains neutral with regard to jurisdictional claims in published maps and institutional affiliations.